Nanoscale

PAPER

View Article Online
View Journal | View Issue

Cite this: *Nanoscale*, 2016, **8**, 13273

Wall-like hierarchical metal oxide nanosheet arrays grown on carbon cloth for excellent supercapacitor electrodes†

Zongyu Huang,‡[a,b] Zhen Zhang,‡[b] Xiang Qi,[a,b] Xiaohui Ren,[b] Guanghua Xu,[b] Pengbo Wan,*[c] Xiaoming Sun[c] and Han Zhang*[a]

Received 18th May 2016,
Accepted 6th June 2016

DOI: 10.1039/c6nr04020a

www.rsc.org/nanoscale

Recently, considerable efforts have been made to satisfy the future requirements of electrochemical energy storage using novel functional electrode materials. Binary transition metal oxides (BTMOs) possess multiple oxidation states that enable multiple redox reactions, showing higher supercapacitive properties than single component metal oxides. In this work, a facile hydrothermal method is provided for the synthesis of wall-like hierarchical metal oxide $MMoO_4$ (M = Ni, Co) nanosheet arrays, which are directly grown on flexible carbon cloth for use as advanced binder-free electrodes for supercapacitors. By virtue of their intriguing structure, the resulted active material nanosheets with a high specific surface area can provide a large electroactive region, which could facilitate easy accession of electrolyte ions and fast charge transport, resulting in an enhanced electrochemical performance. Separately, the as-synthesized $MMoO_4$ (M = Ni, Co) samples have exhibited superior specific capacitances (1483 F g^{-1} of $NiMoO_4$ and 452 F g^{-1} of $CoMoO_4$ at a current density of 2 A g^{-1}), as well as excellent cycling stability (93.1% capacitance retention of $NiMoO_4$ and 95.9% capacitance retention of $CoMoO_4$ after 2000 cycles). The results show that the binder-free electrodes constructed by deposition of $MMoO_4$ (M = Ni, Co) nanosheets on carbon cloth are promising candidates for the application of supercapacitors.

Introduction

Recently, a significant amount of effort has been devoted to the investigation of high-performance, low-cost and environmentally friendly energy-storage systems, in order to meet the requirements of rapid development of portable electronic devices and electrical vehicles. As one of the most important electrochemical energy storage technologies, supercapacitors (SCs), also named electrochemical capacitors (ECs), have triggered worldwide attention, due to their excellent features of fast recharge ability, high power performance, a long cycle life and environmental friendliness.[1–5] Generally, according to their mode of charge-storage mechanisms, SCs are usually grouped into two categories: electrical double-layer capacitors (EDLCs), in which the capacitance is generated from the accumulated charge physically stored on the electrode surface *via* adsorbing–desorbing charged ions from the electrolyte onto the electrode surfaces, and redox electrochemical capacitors, also called pseudocapacitors, resulting from the fast and reversible redox reactions between the electrolyte and electrode materials on the electrode surface.[6] Regarded as typical EDLCs, carbon-based materials including graphene,[7] carbon nanotubes,[8] active carbon[9] and mesoporous carbon[10] have been extensively investigated. Unfortunately, because there is no electrochemical reaction between the electrode of carbon and the electrolyte, the relatively low specific capacitance of EDLCs has seriously limited their practical use in SCs. Thus, various kinds of pseudocapacitive materials possessing reversible redox reactions have long been promising alternative materials to carbon-based materials.[11–13]

Although a lot of progress has been made in pseudocapacitive electrode materials for SCs, high cost (*e.g.* RuO_2-based materials) and harm to the environment (*e.g.* metal sulfide) are still the obstacles to the development of SCs.[14,15] As a

[a]*SZU-NUS Collaborative Innovation Center for Optoelectronic Science and Technology, Shenzhen Key Laboratory of Two-Dimensional Materials and Devices and Key Laboratory of Optoelectronic Devices and Systems of Ministry of Education and Guangdong Province, Shenzhen University, Shenzhen, P. R. China. E-mail: hzhang@szu.edu.cn*
[b]*Hunan Key Laboratory of Micro-Nano Energy Materials and Devices, Laboratory for Quantum Engineering and Micro-Nano Energy Technology and School of Physics and Optoelectronics, Xiangtan University, Hunan 411105, P. R. China*
[c]*State Key Laboratory of Chemical Resource Engineering, P.O. Box 98, Beijing University of Chemical Technology, Beijing 100029, P.R. China. E-mail: pbwan@mail.buct.edu.cn*

†Electronic supplementary information (ESI) available: XRD pattern and charge–discharge plots. See DOI: 10.1039/c6nr04020a

‡These authors contributed equally.

group of promising and low cost pseudocapacitive materials, binary transition metal oxides (BTMOs) possessing multiple oxidation states have exhibited superior electrochemical performance to single component metal oxides because of their feasible oxidation states and better electrical conductivity.[16,17] In particular, binary transition metal molybdates, such as $NiMoO_4$ and $CoMoO_4$, are gradually being studied for high performance pseudocapacitor electrodes due to their abundant resource, high availability and environmental friendliness. For example, Jiang *et al.* successfully prepared $NiMoO_4{\cdot}H_2O$ nanoclusters for supercapacitors by rapid microwave-assisted synthesis, which showed a specific capacitance value of 682 F g^{-1} at the current density of 0.5 A g^{-1}.[18] Liu *et al.* reported a hydrothermal process to fabricate one-dimensional $CoMoO_4{\cdot}0.9H_2O$ nanorods, which exhibited a specific capacitance of 326 F g^{-1} at the current density of 5 mA cm^{-2}.[19] Despite this progress, however, it is highly desirable to design and fabricate $MMoO_4$ (M = Ni, Co) materials *via* a more facile and simple approach for achieving higher electrochemical performance.

Generally, it is well documented that a well-defined hierarchical nanostructure assembled from two-dimensional nanosheets has been considered as a promising structure in the field of energy storage, which can greatly improve the electrode/electrolyte contact area, increase the amount of electroactive sites and allow the ion and electron transport.[20] In order to increase the conductivity of the electrode, growing a well-designed hierarchical structure on the conductive substrate is an emerging efficient strategy.[21] As a soft substrate, carbon cloth not only enables easy diffusion of the electrolyte and numerous fast electro-transport accesses, but also avoids the use of a polymer binder and an additional slurry-coating procedure, fully eliminating the contact resistance between the current collector and the active materials. Hence, the controllable fabrication of hierarchical metal molybdate nanosheets directly grown on a flexible carbon cloth substrate for use as binder-free supercapacitor electrodes is imperative but remains a great challenge.

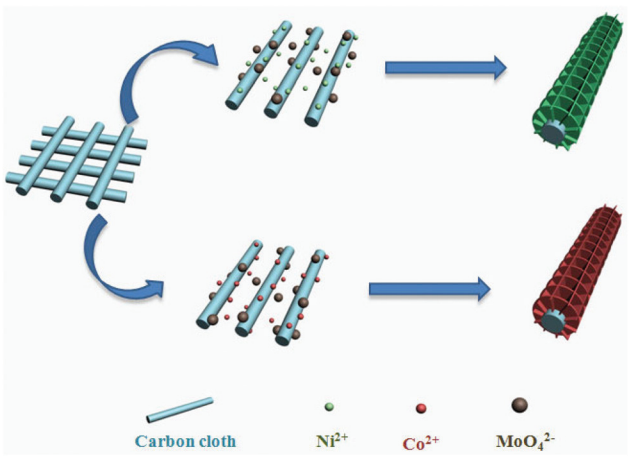

Fig. 1 Schematic illustration of the formation mechanism of $NiMoO_4$ and $CoMoO_4$ nanosheets.

In the present work, we report the facile hydrothermal synthesis of $MMoO_4$ (M = Ni, Co) nanosheets on conductive carbon cloth, which is directly used as binder-free electrodes for electrochemical capacitors (Fig. 1). The as-prepared samples exhibit satisfactory capacitances (1483 F g^{-1} of $NiMoO_4$ and 452 F g^{-1} of $CoMoO_4$ at a current density of 2 A g^{-1}), remarkable rate capability (943 F g^{-1} of $NiMoO_4$ and 356 F g^{-1} of $CoMoO_4$ at a current density up to 12 A g^{-1}) and a good cycling stability (93.1% and 95.9% capacitance retention after 2000 cycles in a 1 M KOH aqueous electrolyte), making them one of the most promising, effective and scalable alternatives for SCs.

Experimental

Materials

All the chemicals are of analytical grade. Nickel nitrate hydrate ($Ni(NO_3)_2{\cdot}6H_2O$), cobalt nitrate hydrate ($Co(NO_3)_2{\cdot}6H_2O$) and sodium molybdate hydrate ($Na_2MoO_4{\cdot}2H_2O$) are purchased from Aladdin. Carbon cloth is brought from Taiwan Ce Tech Co. All the chemicals are used as received without further purification. Deionized (DI) water from Millipore Q is used throughout the whole experiment. And all aqueous solutions were prepared with ultrapure water.

Synthesis of $MMoO_4$ nanosheets

Prior to the synthesis, the carbon cloth substrate is cleaned with acetone, 10% hydrogen nitrate and DI water respectively with the assistance of ultrasonication for several minutes before the hydrothermal reaction and then placed standing against the wall of a Teflon-lined autoclave. The reaction solution is obtained by mixing 10 mM $Ni(NO_3)_2{\cdot}6H_2O$ and 10 mM ($Na_2MoO_4{\cdot}2H_2O$) in 20 mL DI water under constant magnetic stirring for 30 minutes and then transferred into a Teflon-lined autoclave. The autoclave is sealed and maintained at 150 °C for 6 h and then allowed to cool to room temperature. After the reaction, the carbon cloth is taken out and washed with DI water followed by ethanol in order to remove the residual impurities, and then dried in an oven at 60 °C for 12 h. Finally, the carbon cloth with as-grown active materials is annealed at 300 °C for 2 h under a pure argon atmosphere to obtain $NiMoO_4$ nanosheets.

Similarly to the preparation procedure of $NiMoO_4$, $CoMoO_4$ is also synthesized by hydrothermal reaction with a solution of 10 mM $Co(NO_3)_2{\cdot}6H_2O$ and 10 mM $Na_2MoO_4{\cdot}2H_2O$ in 20 mL DI water, which is sealed and maintained at 180 °C for 8 h. Finally, the as-prepared hydrate precursor is annealed at 300 °C for 2 h to obtain the $CoMoO_4$ nanosheets.

Structural characterization

The crystal structures of the as-prepared samples were determined by X-ray diffraction (XRD) using Cu Kα radiation. The morphologies and microstructures of the samples were characterized using scanning electron microscopy (SEM, JEOL, JSM 6360). Raman spectra were collected by using a Renishaw

InVia Raman microscope by excitation at room temperature at an excitation laser wavelength of 532 nm.

Electrochemical tests

The electrochemical properties of the as-obtained electrode material are investigated in a three-electrode configuration where the carbon cloth covered with $NiMoO_4$ and $CoMoO_4$ nanosheets is directly used as the working electrode, and platinum foil and Ag/AgCl served as counter and reference electrodes, respectively. All the electrochemical measurements including cyclic voltammetry, and galvanostatic charge/discharge test are carried out in 1 M KOH aqueous solution with a CHI660D (ChenHua, China) electrochemistry workstation. Electrochemical impedance spectroscopy (EIS) measurement is also carried out in the frequency range of 100 kHz–0.01 Hz with a perturbation amplitude of 5 mV.

Results and discussion

Structural and morphology characterization

The fabrication of $MMoO_4$ (M = Ni, Co) nanosheets grown on carbon cloth substrates is schematically illustrated in Fig. 1. Simply, the positive Ni^{2+} and Co^{2+} are attracted to the negative MoO_4^{2-} rapidly, then reacted to form the $MMoO_4$ precursor after the hydrothermal process, and finally dehydrated to $MMoO_4$ (M = Ni, Co) nanosheets by the annealing treatment. The crystal structures of the as-synthesized $NiMoO_4$ and $CoMoO_4$ nanosheets are studied using XRD. Fig. S1† shows the XRD patterns of the pure carbon cloth substrate, where an obvious and broad peak is centred at $2\theta = 27°$, corresponding to the phase of carbon cloth. In order to avoid the strong impact of the carbon cloth substrate on the XRD results, the $NiMoO_4$ and $CoMoO_4$ active materials are scratched from the carbon cloth for XRD analysis, which is shown in Fig. 2(a). The XRD result of $NiMoO_4$ shows various peaks at $2\theta = 14.3°$, 19.0°, 24.0°, 25.4°, 28.9°, 32.9°, 38.8°, 39.4°, 41.3°, 43.9°, 47.5° and 56.7°, respectively, corresponding to the (110), (−201), (021), (−112), (220), (022), (112), (−132), (040), (330), (−204) and (024) facets of $NiMoO_4$ with lattice constants a = 9.566 Å, b = 8.734 Å, c = 7.649 Å, which are in good agreement with JCPDS card no: 86-0361.[17] Apparently, several diffraction angles at $2\theta = 13.2°$, 23.3°, 26.5°, 28.4°, 32.0°, 36.7°, 38.8°, 40.2°, 47.3°, 53.4° and 54.5° can be assigned to the (001), (021), (002), (−311), (−131), (400), (040), (003), (421), (−441) and (−440) crystal planes, which are attributed to β-$CoMoO_4$ (JCPDS card no: 21-0868, a = 10.210 Å, b = 9.268 Å, c = 7.022 Å), respectively.[22] Fig. 2(b) shows the Raman spectra of the carbon cloth substrate, $NiMoO_4$ and $CoMoO_4$ nanosheets. Obviously, the pure carbon cloth displays two strong and broad peaks at around 1350 cm^{-1} and 1600 cm^{-1}, belonging to the phonon modes of the carbon material.[23] The Raman spectrum of pure $CoMoO_4$ exhibits bands at around 939 cm^{-1}, 863 cm^{-1} and 368 cm^{-1}, corresponding to the Mo–O–Co stretching vibrations in $CoMoO_4$ species, while the bands at 816 cm^{-1} and 337 cm^{-1} can be attributed to MoO_4 vibrations, respectively.[24] As for pure $NiMoO_4$, bands at 857 cm^{-1} and 942 cm^{-1} can be attributed to the symmetric stretching of the Mo–O–Ni bond.[25]

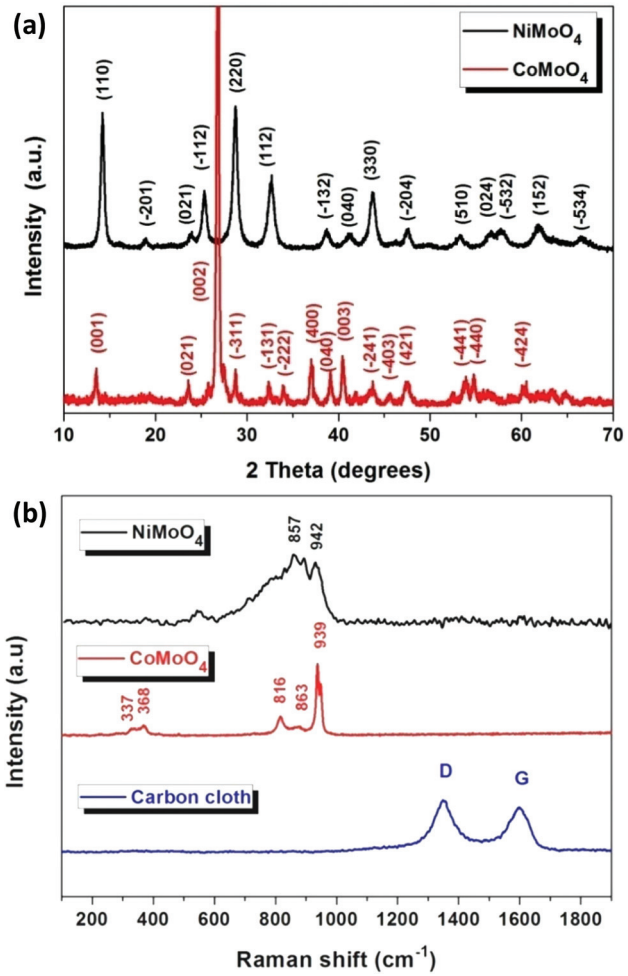

Fig. 2 XRD patterns (a) and Raman spectra (b) of $NiMoO_4$ and $CoMoO_4$ nanosheets.

The SEM images of $MMoO_4$ (M = Ni, Co) nanosheets on carbon cloth substrates are shown in Fig. 3. Notably, as presented in Fig. 3(a and b), it can be seen that the $NiMoO_4$ nanosheets are uniformly grown on the carbon cloth substrate. As can be seen from the enlarged SEM image in Fig. 3(b), these $NiMoO_4$ nanosheets with about 40 nm thickness are almost vertically grown on the substrate, interconnected with each other to form a wall-like structure, revealing a hierarchical array feature, which may allow rapid and effective ion charge transfer and electron transport. Similarly, as indicated in Fig. 3(c and d), nanostructured $CoMoO_4$ products are uniformly distributed on the skeleton of carbon cloth, which presents a larger thickness (about 50 nm) than that of $NiMoO_4$ nanosheets.

Electrochemical performance

To demonstrate the advantage of these electrodes and further explore their potential applications in supercapacitors, cyclic

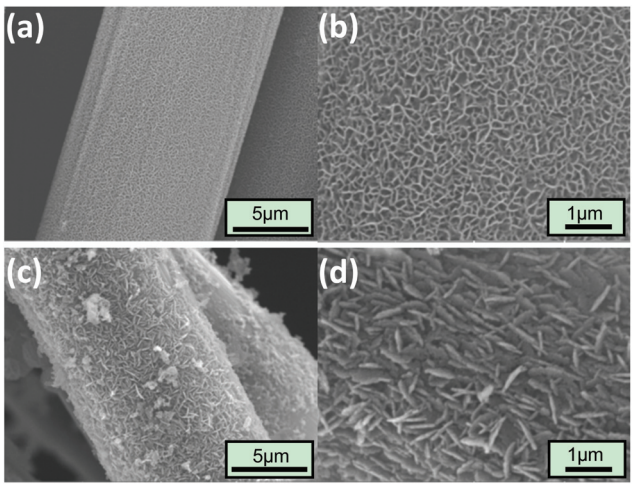

Fig. 3 SEM images for pure $NiMoO_4$ (a, b) and $CoMoO_4$ nanosheets (c, d).

voltammetry (CV), rate capability analysis, cyclic stability studies and electrochemical impedance spectroscopy are conducted in a 1 M KOH aqueous electrolyte. A well-defined redox peak is observed for $NiMoO_4$ nanosheets (Fig. 4(a)), due to

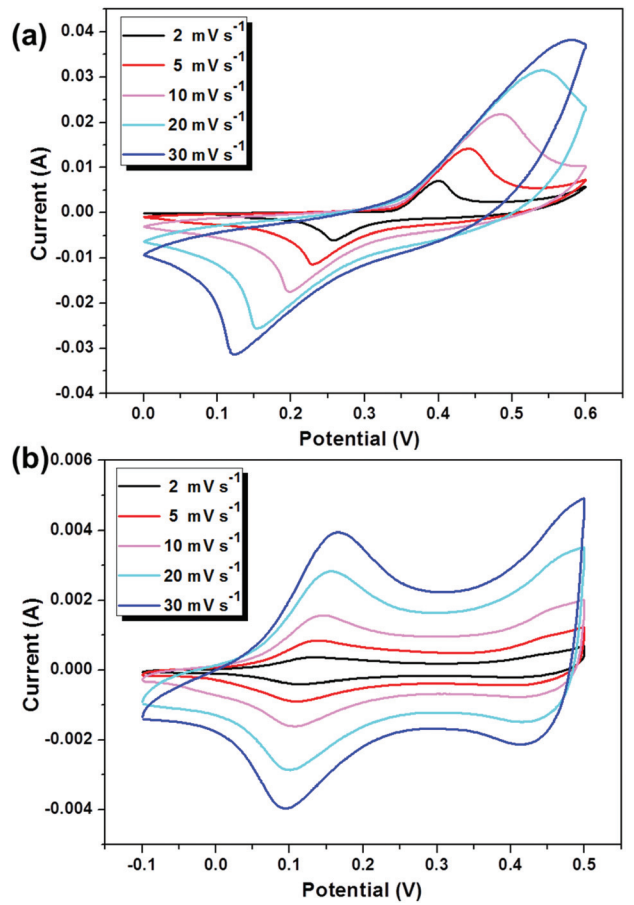

Fig. 4 CV curves of $NiMoO_4$ (a) and $CoMoO_4$ nanosheets (b) at various scan rates ranging from 2 mV s^{-1} to 30 mV s^{-1}.

the following diffusion-controlled reversible Faradaic redox reaction:

$$Ni^{2+} \leftrightarrow Ni^{3+} + e^- \quad (1)$$

in an alkaline electrolyte.[26,27] Notably, a pair of peaks is observed in the CV curves of $CoMoO_4$ nanosheets in the potential region from −0.1 V–0.5 V (Fig. 4(b)), suggesting that the capacitance characteristics are mainly governed by Faradaic reactions, which correspond to the following redox reaction:[28]

$$3[Co(OH)_3]^- \leftrightarrow Co_3O_4 + 4H_2O + OH^- + 2e^- \quad (2)$$

$$Co_3O_4 + H_2O + OH^- \leftrightarrow 3CoOOH^- + e^- \quad (3)$$

$$CoOOH + OH^- \leftrightarrow CoO_2 + H_2O + e^- \quad (4)$$

These features are quite different from those of EDLCs with an ideal rectangular shape, which are usually produced by the electric double-layer capacitance. With the scan rate increase, the anodic peak shifts toward the positive potential and the cathodic peak shifts towards the negative potential. Besides, the peak current increases nearly linearly with the scan rate increase and the shapes of CV curves maintain well even at a high scan rate of 30 mV s^{-1}, indicating that the rates of electronic and ionic transports are rapid enough. Fig. S2† compares the CV curves of the $NiMoO_4$ nanosheets and pure carbon cloth substrate electrode at the scan rate of 10 mV s^{-1}. The current density of $NiMoO_4$ nanosheets is much higher than that for pure carbon cloth, indicating that the contribution to the capacity for the carbon cloth substrate is negligible.

Fig. 5(a and b) represent the galvanostatic charge–discharge curves of $NiMoO_4$ and $CoMoO_4$ products obtained at various current densities ranging from 2 to 12 A g^{-1}. Obviously, well-defined plateaus during the charge–discharge process are observed, suggesting that both $NiMoO_4$ and $CoMoO_4$ have good pseudocapacitive behaviours, which is in agreement with the result of the above CV tests. The capacitances of $NiMoO_4$, and $CoMoO_4$ at different current densities are provided in Fig. 6(a), which are evaluated from the charge–discharge curves according to the equation:[29]

$$C = (I \times \Delta t)/(m \times \Delta V) \quad (5)$$

where C (F g^{-1}) is the specific capacitance of the electrode based on the mass loading of active materials, I (A) is the current during the discharge process, Δt (s) is the discharge time, and ΔV (V) is the potential window. The specific capacitances of $NiMoO_4$ are 1483, 1226, 1123, 1042 and 969 F g^{-1} corresponding to the discharge current densities of 2, 4, 6, 8 and 10 A g^{-1}, respectively. Though the specific capacitance shows a gradual decrease along with the increase of current density, the as-prepared hybrid composite presents a good rate capability. Even at a large current density of 12 A g^{-1}, the $NiMoO_4$ electrode exhibits a specific capacitance of 943 F g^{-1}, nearly 63.5% retention of the initial value. Similarly, the $CoMoO_4$ electrode also exhibits specific capacitances as high as 452, 430, 415, 396, 378 and 356 F g^{-1} at the current

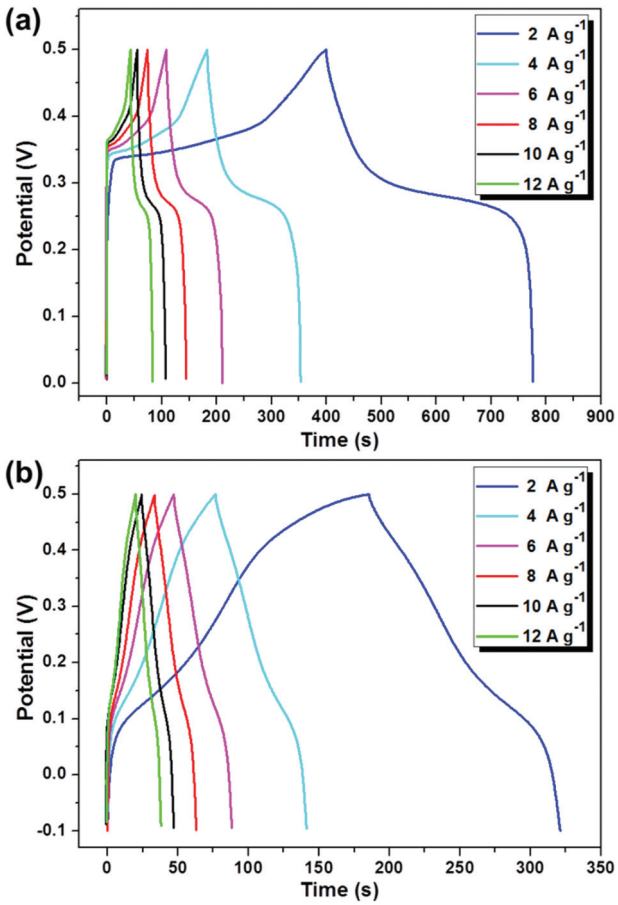

Fig. 5 Galvanostatic charge–discharge curves at different charge–discharge current densities for $NiMoO_4$ (a) and $CoMoO_4$ nanosheets (b).

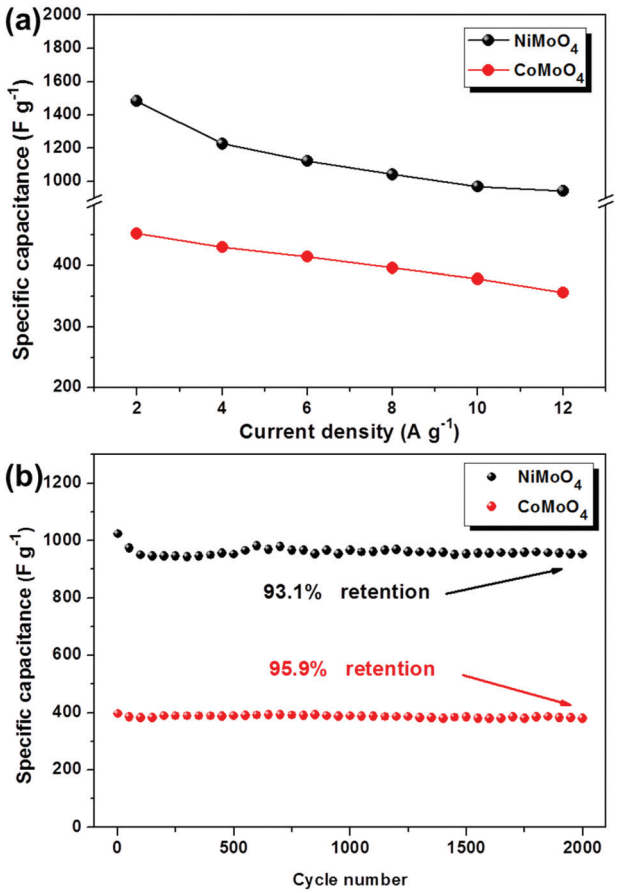

Fig. 6 The specific capacitances of $MMoO_4$ at various current densities (a) and cycling performance at the current density of 8 A g^{-1} over 2000 cycles (b).

densities of 2, 4, 6, 8, 10 and 12 A g^{-1}, respectively. The obtained high specific capacitance and good rate capability are ascribed to the unique interconnected nanosheet architecture, providing abundant space "ion-buffering reservoirs" for ion transport.

Cycling stability is another key performance indicator of supercapacitors. Fig. 6(b) shows the cycling performance of the $NiMoO_4$ and $CoMoO_4$ electrodes at the current density of 8 A g^{-1} over 2000 cycles. The $CoMoO_4$ electrode exhibits excellent electrochemical stability with only 4.1% deterioration of the initial available capacitance after 2000 cycles. Though a slight decrease of capacitance for $NiMoO_4$ in the initial 100 cycles is observed, the specific capacitance still reached 952 F g^{-1}, corresponding to a retention of about 93.1%. EIS measurements are carried out to understand the electrochemical behaviours of $MMoO_4$ (M = Ni, Co) nanosheets. As shown in Fig. 7(a), the Nyquist plots exhibit a depressed semicircle in the high frequency range, followed by a linear slope in the low frequency region, which is called the Warburg resistance resulting from the frequency dependence of ion diffusion/transport in the electrolyte.[30] The equivalent series resistance (ESR) of the electrode can be obtained from the x intercept of the Nyquist plot. The ESR values of the $NiMoO_4$ and $CoMoO_4$ electrodes are 3.48 Ω and 3.59 Ω, respectively. The diameter of the semi-circle corresponds to the charge transfer resistance caused by Faradic reactions in parallel with the double-layer capacitance at the electrode–electrolyte interface.[31–35] According to the enlarged plots, the size of the semicircle, which equals the charge transfer resistance R_{ct}, is smaller for the $NiMoO_4$ electrode (0.8 Ω) compared to that of the $CoMoO_4$ electrode (1.2 Ω), indicating that the binder-free electrode design could greatly improve the conductivity, thus leading to enhanced electrochemical properties.

As described by various characterization methods above, the excellent electrochemical performance of $NiMoO_4$ and $CoMoO_4$ electrodes is mainly due to the following three factors shown in Fig. 7(b): (1) the unique interconnected nanosheet arrays may enlarge the electrode/electrolyte contact areas, greatly shortening the diffusion and migration paths of electrolyte ions, which would contribute to the overall specific capacitance, especially during the rapid charge–discharge process. (2) The high electrical conductivity of metal molybdates enables rapid and effective ion charge transfer and electron transport, favoring the electrochemical behaviours. (3) The direct deposition of the integrated smart architecture on carbon cloth used as a binder-free electrode could ensure good

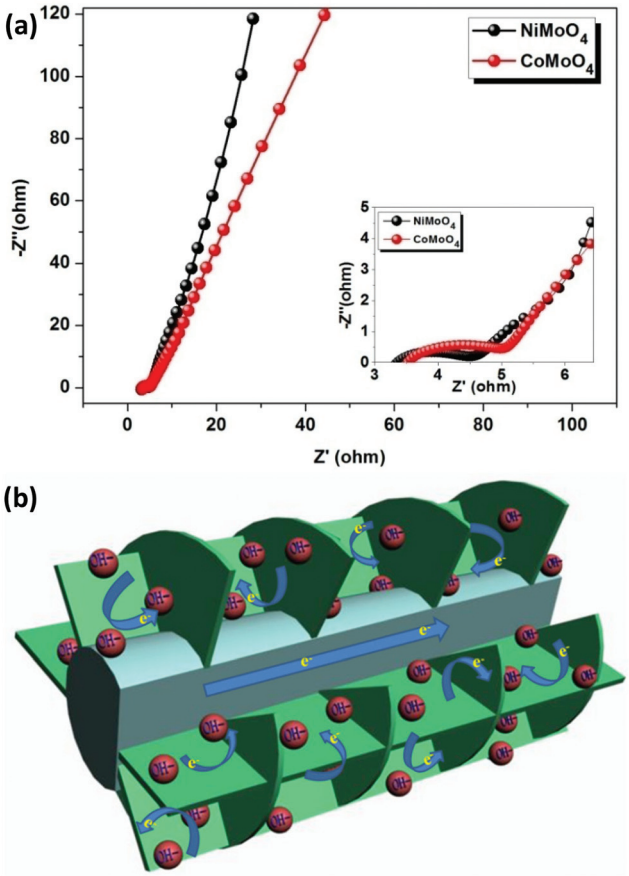

Fig. 7 EIS curves of $NiMoO_4$ and $CoMoO_4$ (a), the inset shows the enlarged plot; schematic of the application advantage of the $MMoO_4$ nanosheets on carbon cloth (b).

mechanical adhesion and good electrical contact with the conductive substrate, thus resulting in an enhanced rate capability. The results clearly show that the as-prepared $MMoO_4$ (M = Ni, Co) nanosheets are very promising electrode materials for supercapacitor application.

Conclusions

In summary, a simple and environmentally friendly hydrothermal synthesis method is presented to fabricate $MMoO_4$ (M = Ni, Co) nanosheets on the carbon cloth substrate for direct use as binder-free electrodes with high electrochemical performance for supercapacitors. The as-prepared nanocomposites exhibit high capacitance (1483 F g^{-1} of $NiMoO_4$ and 452 F g^{-1} of $CoMoO_4$ at a current density of 2 A g^{-1}), good rate capability (943 F g^{-1} of $NiMoO_4$ and 356 F g^{-1} of $CoMoO_4$ at a high current density of 12 A g^{-1}) and excellent cycling stability (93.1% capacitance retention of $NiMoO_4$ and 95.9% capacitance retention of $CoMoO_4$ after 2000 cycles). Such superior capacitive behavior is ascribed to the hierarchical nanostructure assembled from two-dimensional nanosheets and the direct growth of active materials on the conducting carbon cloth substrate as binder-free electrodes. The remarkable electrochemical properties should make the present $NiMoO_4$ and $CoMoO_4$ nanosheets excellent electrode materials for supercapacitors.

Acknowledgements

This work was supported by the grants from the National Natural Science Foundation of China (no. 61435010, 11504312 and 61490713), the Open Fund based on the Innovation Platform of Hunan Colleges and Universities (no. 15K128), the Provincial Natural Science Foundation of Hunan (no. 14JJ3079), the Key laboratory of Optoelectronic Devices and Systems of Ministry of Education and Guangdong Province Fund (no. GD201404), the Science and Technology Innovation Commission of Shenzhen (KQTD20150324162703 85), and the Science and Technology Innovation Commission of Shenzhen (JCYJ20150625103619275).

Notes and references

1 Q. Lu, J. G. Chen and J. Q. Xiao, *Angew. Chem., Int. Ed.*, 2013, **52**, 1882–1889.
2 Z. Yu, L. Tetard, L. Zhai and J. Thomas, *Energy Environ. Sci.*, 2015, **8**, 702–730.
3 Y. Yang, H. Wang, R. Hao and L. Guo, *Small*, 2016, DOI: 10.1002/smll.201503924.
4 H. Wang, F. Li, B. Zhu, L. Guo, Y. Yang, R. Hao, H. Wang, Y. Liu, W. Wang and X. Guo, *Adv. Funct. Mater.*, 2016, **26**, 3472–3479.
5 H. Wang, B. Zhu, W. Jiang, Y. Yang, W. R. Leow, H. Wang and X. Chen, *Adv. Mater.*, 2014, **26**, 3638–3643.
6 C. Liu, Z. Yu, D. Neff, A. Zhamu and B. Z. Jang, *Nano Lett.*, 2010, **10**, 4863–4868.
7 C. X. Guo and C. M. Li, *Energy Environ. Sci.*, 2011, **4**, 4504–4507.
8 D. N. Futaba, K. Hata, T. Yamada, T. Hiraoka, Y. Hayamizu, Y. Kakudate, O. Tanaike, H. Hatori, M. Yumura and S. Iijima, *Nat. Mater.*, 2006, **5**, 987–994.
9 D. Pech, M. Brunet, H. Durou, P. Huang, V. Mochalin, Y. Gogotsi, P. L. Taberna and P. Simon, *Nat. Nanotechnol.*, 2010, **5**, 651–654.
10 W. Li, F. Zhang, Y. Dou, Z. Wu, H. Liu, X. Qian, D. Gu, Y. Xia, B. Tu and D. Zhao, *Adv. Energy Mater.*, 2011, **1**, 382–386.
11 H. Wang, H. S. Casalongue, Y. Liang and H. Dai, *J. Am. Chem. Soc.*, 2010, **132**, 7472–7477.
12 Q. Yang, Z. Lu, T. Li, X. M. Sun and J. F. Liu, *Nano Energy*, 2014, **7**, 170–178.
13 C. C. Hu, K. H. Chang, M. C. Lin and Y. T. Wu, *Nano Lett.*, 2006, **6**, 2690–2695.
14 H. Zhang, Y. Li, T. Xu, J. Wang, Z. Huo, P. Wan and X. Sun, *J. Mater. Chem. A*, 2015, **3**, 15020–15023.

15 Z. Lu, W. Zhu, X. Yu, H. Zhang, Y. Li, X. Sun, X. Wang, H. Wang, J. Wang, J. Luo, X. Lei and L. Jiang, *Adv. Mater.*, 2014, **26**, 2683–2687.
16 Y. Zhang, L. Li, H. Su, W. Huang and X. Dong, *J. Mater. Chem. A*, 2015, **3**, 43–59.
17 D. Chen, Q. Wang, R. Wang and G. Shen, *J. Mater. Chem. A*, 2015, **3**, 10158–10173.
18 H. Wan, J. Jiang, X. Ji, L. Miao, L. Zhang, K. Xu, H. Chen and Y. Ruan, *Mater. Lett.*, 2013, **108**, 164–167.
19 M.-C. Liu, L.-B. Kong, X.-J. Ma, C. Lu, X.-M. Li, Y.-C. Luo and L. Kang, *New J. Chem.*, 2012, **36**, 1713–1716.
20 S. Peng, L. Li, H. B. Wu, S. Madhavi and X. W. Lou, *Adv. Energy Mater.*, 2015, **5**, 1401172.
21 G. Q. Zhang, H. Wu, H. Hoster, M. Chan-Park and X. W. Lou, *Energy Environ. Sci.*, 2012, **5**, 9453–9456.
22 D. Guo, H. Zhang, X. Yu, M. Zhang, P. Zhang, Q. Li and T. Wang, *J. Mater. Chem. A*, 2013, **1**, 7247–7254.
23 A. Ferrari, J. Meyer, V. Scardaci, C. Casiraghi, M. Lazzeri, F. Mauri, S. Piscanec, D. Jiang, K. Novoselov and S. Roth, *Phys. Rev. Lett.*, 2006, **97**, 187401.
24 T. Yang, H. Zhang, L. Mei, D. Guo, Q. Li and T. Wang, *Electrochim. Acta*, 2015, **158**, 327–332.
25 J. Haetge, I. Djerdj and T. Brezesinski, *Chem. Commun.*, 2012, **48**, 6726–6728.
26 D. Cai, B. Liu, D. Wang, Y. Liu, L. Wang, H. Li, Y. Wang, C. Wang, Q. Li and T. Wang, *Electrochim. Acta*, 2014, **115**, 358–363.
27 L.-Q. Mai, F. Yang, Y.-L. Zhao, X. Xu, L. Xu and Y.-Z. Luo, *Nat. Commun.*, 2011, **2**, 381.
28 X. Yu, B. Lu and Z. Xu, *Adv. Mater.*, 2014, **26**, 1044–1051.
29 X.-J. Ma, L.-B. Kong, W.-B. Zhang, M.-C. Liu, Y.-C. Luo and L. Kang, *Electrochim. Acta*, 2014, **130**, 660–669.
30 M. D. Stoller, S. Park, Y. Zhu, J. An and R. S. Ruoff, *Nano Lett.*, 2008, **8**, 3498–3502.
31 K. Wang, P. Zhao, X. Zhou, H. Wu and Z. Wei, *J. Mater. Chem.*, 2011, **21**, 16373–16378.
32 Z. Niu, P. Luan, Q. Shao, H. Dong, J. Li, J. Chen, D. Zhao, L. Cai, W. Zhou, X. Chen and S. Xie, *Energy Environ. Sci.*, 2012, **5**, 8726–8733.
33 H. Cong, X. Ren, P. Wang and S. H. Yu, *Energy Environ. Sci.*, 2013, **6**, 1185–1191.
34 Y. Xu, G. Shi and X. Duan, *Acc. Chem. Res.*, 2015, **48**, 1666–1675.
35 C. G. Hu, L. Song, Z. P. Zhang, N. Chen, Z. H. Feng and L. T. Qu, *Energy Environ. Sci.*, 2015, **8**, 31–54.